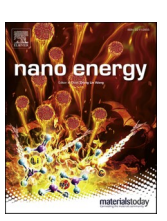


Contents lists available at ScienceDirect

# Nano Energy

journal homepage: http://www.elsevier.com/locate/nanoen





# Sorting-free utilization of semiconducting carbon nanotubes for large thermoelectric responses

Jui-Hung Hsu<sup>a</sup>, Choongho Yu<sup>a,b,\*</sup>

- <sup>a</sup> Department of Materials Science and Engineering, Texas A&M University, College Station, TX, 77843, USA
- <sup>b</sup> Department of Mechanical Engineering, Texas A&M University, College Station, TX, 77843, USA

#### ARTICLE INFO

Keywords: Thermoelectric Carbon nanotube PEDOT:PSS Junction Semiconducting Metallic

#### ABSTRACT

Semiconducting carbon nanotubes (s-CNTs) are promising organic thermoelectric materials mainly due to their large thermopower (or Seebeck coefficient), but it is impractical to pick only s-CNTs out of a mixture of different chirality tubes in mass-produced CNTs. Here we report a sorting-free method for getting the large thermopower by suppressing electronic transport from metallic CNT (m-CNT). This study employed an organic electrochemical transistor (OECT) configuration where poly (3,4-ethylenedioxythiophene): poly (styrenesulfonate) (PEDOT:PSS) channel was disposed between two separated CNT films. Based on the experimentally constructed band diagrams and theoretical estimation, the PEDOT:PSS channel could create energy barriers for abating the contribution of m-CNT to thermopower as well as injecting holes to CNT films. As the gate bias voltage was raised up to 20 V, thermopower was noticeably increased, resulting in the maximum power factor. For practical applications without an externally supplied bias voltage, nanoscale PEDOT:PSS were deposited on top of one end of CNT films for the out-of-plane hole transport, and then PEDOT:PSS was chemically de-doped to adjust the Fermi level like the OECT experiment. With six CNT-PEDOT connections, the thermopower was raised up to  $\sim$ 150  $\mu$ V/K and a remarkably high PF was obtained up to  $\sim 1.3 \times 10^3 \, \mu \text{W/m-K}^2$  at room temperature, which is  $\sim 460\%$  improvement compared with that of pristine CNT and is comparable to those of inorganic counterparts. This study provides not only better understanding of thermoelectric behaviors for organic thermoelectric materials, but also a practical method for suppressing the electronic transport from m-CNT, which would be widely applicable to other organic materials for thermoelectrics and beyond.

# 1. Introduction

Thermoelectric generator utilizes the Seebeck effect to convert thermal energy directly into electricity without moving parts and working fluids. Low-grade heat such as heat from humans and power consuming devices, which is otherwise wasted, could be utilized to power distributed small electronic devices. Recently fully organic thermoelectric materials have been of great interest because of the potentials in delivering power to wearable electronics and the internet-of-things (IoT) with benefits of mechanical flexibility, lightweight, disposability, easy manufacturing, and low cost, compared with the inorganic thermoelectric materials [1–8]. The most popular organic materials are conducting polymers such as poly (3,4-ethylenedioxythiophene):polystyrene sulfonate (PEDOT:PSS) and polyaniline (PANI) due to the relatively high electrical conductivity [9–11]. The conducting polymers, however, are rather brittle and mechanically weak, and their properties

degrade over time in ambient conditions.

Carbon nanotubes (CNTs) have the benefit of the conducting polymers including high electrical conductivity and lightweight, and additionally provide mechanical robustness and stability. Nevertheless CNTs have often been excluded for thermoelectric applications mainly due to the intrinsically high thermal conductivity of "individual" CNTs [12]. The thermoelectric performance of a material is inversely proportional to thermal conductivity according to the dimensionless figure-of-merit called  $ZT = S^2 \sigma T/\kappa$ , where S,  $\sigma$ ,  $\kappa$ , T stand for thermopower (or Seebeck coefficient), electrical conductivity, thermal conductivity, and absolute temperature, respectively. The high thermal conductivity of individual CNTs is suppressed when many CNTs are made into bulks or films because of large thermal contact resistances at the junctions between CNTs [13]. Here CNTs often make point and line contacts, resulting in large thermal contact resistances. For example, the thermal conductivity of CNT films along the out-of-plane direction can be as low

<sup>\*</sup> Corresponding author. Departments of Mechanical Engineering, Materials Science and Engineering, Texas A&M University, College Station, TX, 77843, USA. E-mail address: chyu@tamu.edu (C. Yu).

as 0.1-0.2 W/m-K [14]. It has been also found that the thermal conductivity of CNT films can be significantly reduced by making polymer composites because polymers intervene in the thermal transport between CNTs [15,16].

The junction can also significantly affect the electrical properties, which are indicated by the numerator of ZT,  $S^2\sigma$  called the power factor (PF). In fact, the electrical properties govern the thermal-to-electrical energy conversion so the PF is the most important parameter in thermoelectric materials. It has been shown that the PF of CNT can be widely changed by dispersants mainly because the size of the CNT bundles and contacts between CNTs are different [17]. With more de-bundled CNTs, the contact surfaces between CNTs are larger with less pores, and the electrical conductivity gets higher.

The interposed polymers can affect the electrical transport positively or negatively depending on the properties and characteristics of the polymers. Although quite a few papers about polymer-CNT composites have been recently published [18-20], the aforementioned interesting behaviors have not been rigorously studied. In fact, this study is quite complicated because as-grown CNTs consist of both semiconducting and metallic tubes with various chirality. Interestingly a recent study have shown that semiconducting CNTs (s-CNTs) with controlled chirality distribution and carrier density yielded a high PF. It was reported that s-CNTs have higher thermopower than those of metallic CNTs (m-CNTs) and unsorted CNTs, significantly improving the PF up to  $\sim 110 \,\mu\text{W/m-K}^2$ for s-CNT with uncontrolled chirality [21] and  $\sim 340 \,\mu\text{W/m-K}^2$  for controlled chirality and carrier density [22]. These results have demonstrated that s-CNTs could be a very promising thermoelectric material, but arduous sorting of specific s-CNTs out of as-grown CNTs precludes them as practical thermoelectric materials.

Herein we report a method of attaining the transport properties of s-CNTs without sorting them from a mixture of s-CNT and m-CNT. Controllable junctions between CNTs were designed so as to selectively allow electrical transport from s-CNT using energy barriers whose heights were modulated using an organic electrochemical transistor (OECT) configuration by serially connecting CNT, PEDOT:PSS, and CNT. The gate bias voltage can reversibly dope or de-dope PEDOT:PSS so as to vary the Fermi level, and thereby change the energy barrier height. The thermopower and electrical conductivity were measured, and their behaviors were analyzed in conjunction with the barrier heights obtained from the energy band diagrams constructed by multiple characterization techniques. Similar concepts have been implemented using chemical dedoping of PEDOT:PSS for practical applications instead of the OECT configuration requiring a gate voltage.

#### 2. Results and discussion

## 2.1. Enlarging thermopower by selective transport through s-CNT

Unsorted CNTs consist of various chirality, and the electronic density of states (DOS) vary depending on the chirality. Typical CNT films contain millions of CNTs with various chirality, and the electrical properties in experiments come from average collective behaviors. Despite the complexity, it is notable that m-CNT has non-zero, continuous DOS in contrast to s-CNT. For example, the DOS of semiconducting (9,4), (12,1), (13,0), and metallic (6,6), (9,9) tubes [23] are overlaid when the middle of the band gap was set to 0 eV in the y-axis, as shown in Fig. 1a. Suppose that these chirality tubes are abundant and DOS are simply added together to see the collective behaviors qualitatively, and then combined DOS can be plotted as depicted in Fig. 1b. Thermopower can be described as [24].

$$S = \frac{1}{qT} \frac{\int E\tau D(E)(\partial f_{FD}/\partial E)(E - E_f)dE}{\int E\tau D(E)(\partial f_{FD}/\partial E)dE} \equiv \frac{\int (E - E_f)\sigma_d(E) \ dE}{\int \sigma_d(E) \ dE}$$
(1)

where q, T, E,  $E_f$ , D(E),  $\tau$ ,  $f_{FD}$ , and  $\sigma_d$  indicate electron elementary charge, absolute temperature, energy, the Fermi energy, DOS, relaxation time, the Fermi-Dirac distribution, and differential electrical conductivity, respectively. When the relaxation time is approximated as  $\tau = \tau_0 E^r$ , where r = -0.5 under the assumption that scattering due to acoustic phonons is dominant [8,25]. The differential electrical conductivity can be calculated as Fig. 1c assuming that the Fermi level is located at 0.3 eV from the middle of the band gap. The integrand of the numerator in thermopower (Eq. (1)) is plotted in Fig. 1d. The shaded area in red on the left is negative, and that in blue on the right is positive. The numerator of thermopower is the summation of the two shaded areas. Thus, thermopower becomes larger when the electronic carriers corresponding to the negative part — which mainly comes from m-CNT — do not participate in the electronic transport, as conceptually illustrated in Fig. 1e. The following experiment is to test the feasibility of improving the PF by suppressing the contribution of m-CNT in electrical transport.

# 2.2. Design of experiments with organic electrochemical transistors

Here we designed a PEDOT:PSS channel between two in-line CNT films (Fig. 2a), and then poly (4-styrenesulfonic acid) (PSSH) was sprayed on the PEDOT:PSS to create an OECT (Fig. 2b). Fig. 1c schematically illustrates a stacked configuration of PEDOT:PSS and PSSH. The gate bias alters the Fermi level of the PEDOT:PSS, which changes the electronic transport through the channel. We tested three kinds of CNTs, single-wall CNT (SWCNT), double-wall CNT (DWCNT), and multi-wall

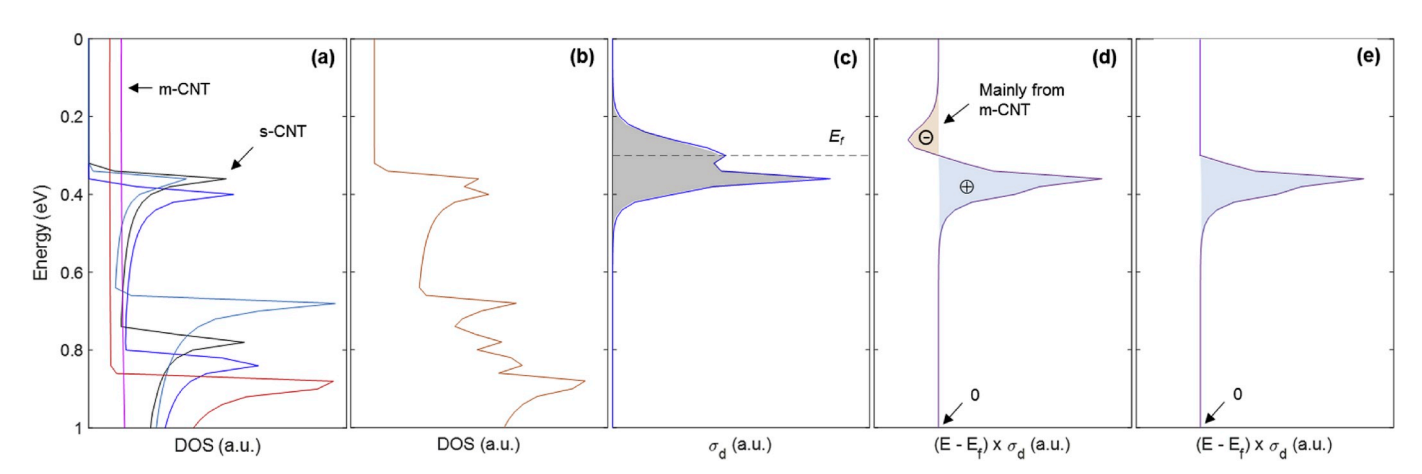


**Fig. 1.** (a) The density of states (DOS) for m-CNTs whose chirality is (6,6) and (9,9), and s-CNT with (9,4), (12,1), and (13,0). The middle of band gap is set to 0 eV and a half DOS is shown for clarity. (b) The summation of the DOS from the tubes in (a). (c) The differential electrical conductivity,  $\sigma_d$ . (d) The integrand of the numerator in thermopower. (e) The integrand of the numerator in thermopower without the contribution from m-CNT.

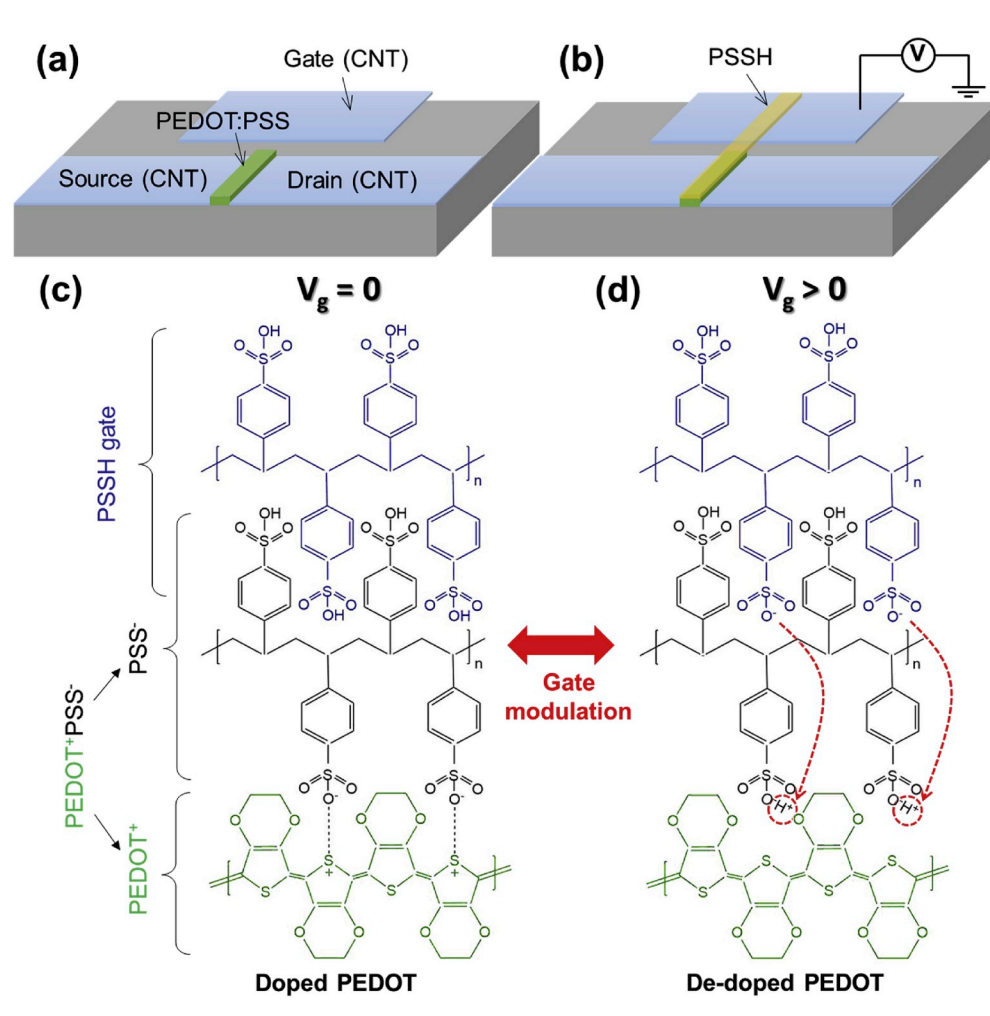


Fig. 2. The OECT fabrication process (not to scale): (a) source, drain, and gate electrodes made of CNT and PEDOT:PSS channel connecting the source and drain, and (b) PSSH gate for bias voltage modulation. The substrate is orders of magnitude thicker than the CNT and PEDOT:PSS films so that temperature profile is linear along the source-todrain direction when thermopower was measured. Illustrations showing the PEDOT: PSS channel with the PSSH gate when the gate bias  $(V_g)$  is (c) 0 V and (d) greater than 0 V.

CNT (MWCNT) whose bandgaps, Fermi levels, and electrical properties are different. Note that typical purified grade CNTs are mixtures of various diameter and length tubes. The device is designed to have longer CNT regions (30 mm  $\times$  2 = 60 mm) than the PEDOT:PSS (3 mm) so that the source-to-drain electrical properties mainly come from CNT rather than PEDOT:PSS. The electrical conductivities of PEDOT and CNT are comparable (Fig. S7).

The PEDOT in PEDOT:PSS is initially doped by the counter PSS<sup>-</sup>, which is indicated by PEDOT<sup>+</sup>PSS<sup>-</sup> in Fig. 1c. When a positive gate voltage ( $V_g > 0$ ) is applied, H<sup>+</sup> in PSSH is repelled and then coupled with the negatively charged PSS<sup>-</sup> in PEDOT:PSS [26], which can be described by the following reaction.

$$PEDOT^{+}PSS^{-} + H^{+} + e^{-} \xrightarrow{V_{g}>0} PEDOT^{0} + H^{+}PSS^{-}$$
 (2)

The  $H^+$  coupled with PSS $^-$  de-dopes PEDOT $^+$  by electron injection (Fig. 1d). The reduced hole doping concentration of PEDOT shifts the Fermi level.

# 2.3. Determination of the Fermi level and band edges

The main contributors for altering electrical conductivity and thermopower with the gate bias are the Fermi level (*i.e.*, doping concentration) and electronic band locations. Therefore, to understand the thermoelectric transport through the source-to-drain, the Fermi level and band edges were experimentally obtained. The highest occupied molecular orbital (HOMO) and the lowest unoccupied molecular orbital (LUMO) were determined by cyclic voltammetry (CV) measurements, as shown in Fig. 3a for SWCNT, Fig. 3b for PEDOT:PSS, and Fig. S2 for

DWCNT. HOMO/LUMO of SWCNT, DWCNT, and PEDOT:PSS were estimated to be 5.03/4.36 eV, 4.91/4.51 eV, and 4.83/3.98 eV, respectively. The bandgap (0.67 eV) for SWCNT is larger than that (0.4 eV) of DWCNT whose diameter is larger than SWCNT. The bandgaps ( $E_{gap}$ ) are close to the values predicted by  $E_{gap}{\approx}0.839~{\rm eV}/d_{\rm CNT}$  (nm) [27], where  $d_{\rm CNT}$  is the diameter of CNT, and they are estimated to be 0.56 eV for SWCNT and 0.37 eV for DWCNT (mean  $d_{\rm SWCNT} \sim 1.5~{\rm nm}$ ; mean  $d_{\rm DWCNT} \sim 2.25~{\rm nm}$  according to the manufacturers' specifications).

The CNT and PEDOT are all p-type materials so the locations of HOMO are crucial. To confirm the HOMO level, ultraviolet photoelectron spectroscopy (UPS) was used, and the cut-off and onset regions of the UPS spectra are shown in Fig. 3c and d for SWCNT and PEDOT:PSS, respectively, and Fig. S3 for DWCNT and MWCNT. The Fermi ( $E_F$ ) and HOMO ( $E_{HOMO}$ ) levels were determined by  $|E_F| = |h\nu - E_{cutoff}|$  and  $|E_{HOMO}| = |h\nu - (E_{cutoff} - E_{onset})|$ , where  $E_{cutoff}$  is the crossover point of the sloping line and x-axis,  $E_{onset}$  is the onset binding energy of the spectra, and  $h\nu$  is the energy of the incident photon.  $E_F$  and  $E_{HOMO}$  of SWCNT from UPS were found to be 5.02 eV and 5.00 eV, respectively. The HOMO of SWCNT is close to that of CV results (5.03 eV). The HOMO levels of PEDOT:PSS from CV (4.83 eV) and UPS (4.81 eV) are also similar.

As the Fermi level is one of the key parameters to determine the energy barrier for the electronic carriers, we used another technique, Kelvin probe force microscopy (KPFM) to cross-check the Fermi level. The work function of a sample ( $WF_{sample}$ ) can be determined by  $WF_{sample} = WF_{tip} - CPD_{sample}$ , where CPD is a contact potential difference between the probe tip and a targeted material. The work function of the microscope probe tip ( $WF_{tip}$ ) was calibrated using pure gold as a reference,  $WF_{tip} = WF_{Au} + CPD_{Au}$ . Fig. 3e shows the CPD profiles of PEDOT:

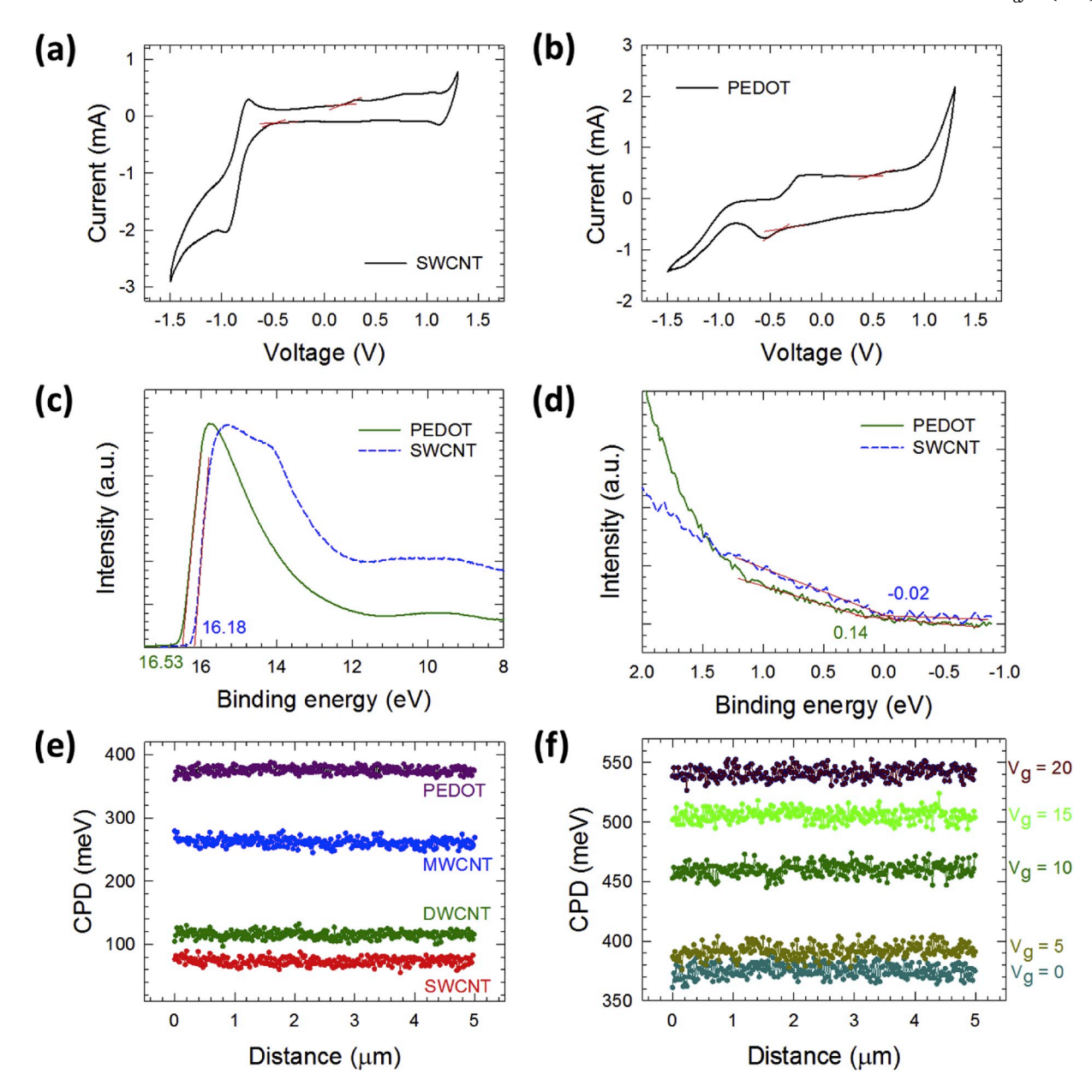


Fig. 3. Cyclic voltammograms for (a) SWCNT and (b) PEDOT:PSS. The x-intercepts by the red sloping lines indicate the onset potentials for oxidation and reduction. (c) A cut-off region and (d) an onset region of the UPS spectra for SWCNT and PEDOT. (e) CPD profiles of PEDOT, SWCNT, DWCNT, and MWCNT obtained from KPFM. (f) CPD profiles of PEDOT when the gate voltages of 0, 5, 10, 15, and 20 V were applied.

PSS, SWCNT, DWCNT, and MWCNT, and Fig. 3f shows those of PEDOT: PSS with gate voltages of 0, 5, 10, 15, and 20 V (see Table S1 for the Fermi levels). The Fermi levels obtained by KPFM were close to those obtained by UPS.

The energy levels of PEDOT, SWCNT, DWCNT, MWCNT obtained from CV, UPS, and KPFM are summarized in Fig. 4a. The Fermi level of SWCNT is on its HOMO, and that of DWCNT is located at the inside of the band, which would be one of the reasons that DWCNT showed higher electrical conductivity than SWCNT. MWCNT is metallic (no band gap) and its work function is smaller than SWCNT and DWCNT. The Fermi level of PEDOT:PSS is located within the band gap and is closer to its HOMO, indicating a p-type character. The positive gate voltage shifted the Fermi level toward the middle of the band gap from  $4.68\,\mathrm{eV}$  at  $V_g=0\,\mathrm{V}$  to  $4.52\,\mathrm{eV}$  at  $V_g=20\,\mathrm{V}$ , indicating that the hole carrier concentration was reduced.

With all the experimentally obtained energy levels, the band diagrams of CNT/PEDOT junctions were constructed (Fig. 4b). The energy

barrier height  $(E_b)$  for holes (majority carrier) based on the band diagram can be obtained using:

$$E_b = (\chi_p + E_{g,p}) - \varphi_p - \left[ (\chi_{CNT} + E_{g,CNT}) - \varphi_{CNT} \right]$$
(3)

where  $E_g$  is the band gap energy for the indexed material (p: polymer);  $\varphi$  is the work function; and  $\chi$  is the electron affinity. For metallic tubes, the bracket containing the last three terms becomes zero. When PEDOT:PSS is doped, polaron and bi-polaron states are created within the band gap [28,29]. The absence of pronounced UV–vis–NIR absorption peak from the PEDOT:PSS in this study (Fig. S4) is indicative of the bipolaron states. Therefore the energy barrier height due to the bipolaron bands ( $E_{b,po}$ ) are expected to be smaller than  $E_b$  although the exact location of the bipolaron bands are uncertain, as illustrated in Fig. 4b and c.

# 2.4. Electrical conductivity and thermopower

The electrical conductivity and thermopower of the OECT with

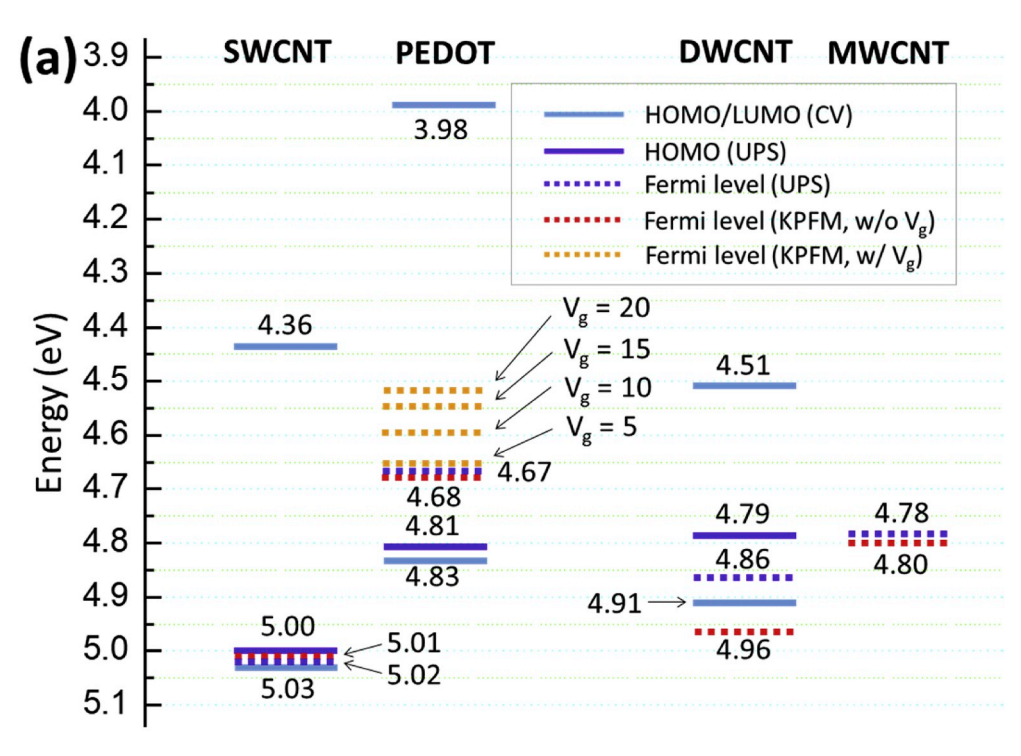
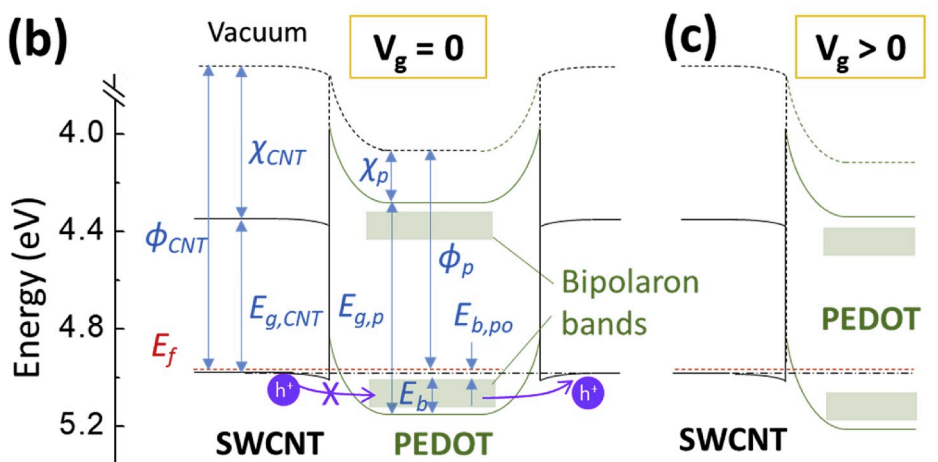


Fig. 4. (a) HOMO, LUMO, and Fermi levels of PEDOT:PSS, SWCNT, DWCNT, and MWCNT determined by CV, UPS, and KPFM. The Fermi levels of PEDOT:PSS were measured when the gate voltage of the OECT was varied from 0 V to 5, 10, 15, and 20 V. (b) The band diagram of SWCNT-PEDOT: PSS-SWCNT junction without gate voltage. Bipolaron bands are indicated by the shaded areas. It is expected that hole transport from SWCNT to PEDOT is suppressed while holes could be injected from PEDOT to SWCNT. (c) The band diagram when  $V_g > 0$  V.



SWCNT (Fig. 5a), DWCNT (Fig. S5a), and MWCNT (Fig. S6a) were measured as a function of gate voltage, and corresponding PF values are shown in Fig. 5b, Fig. S5b, and Fig. S6b, respectively. For comparison, the electrical properties of CNT and PEDOT:PSS were plotted together. When  $V_g=0$  V, the source-to-drain thermopower of SWCNT in the OECT configuration is 78  $\mu$ V/K, which is higher than those of individual components, SWCNT and PEDOT:PSS (Fig. 5a). The extra increment in thermopower apparently indicate that the thermopower does not follow the macroscopic effective medium theory when SWCNTs are connected by PEDOT:PSS. Then the thermopower was further increased to  $124\,\mu$ V/K at  $V_g=15$  V.

We believe that the large increase in thermopower is unlikely to be caused by ionic effects [20] because the thermopower of PEDOT:PSS only sample shows much smaller thermopower values,  $\sim 30~\mu\text{V/K}$ , compared with an extremely large value on the order of  $10^3~\mu\text{V/K}$  with ion dominant cases [20,30–32]. Furthermore, the response time was fast in contrast to slow response due to the sluggish thermally-driven ion transport. When composites were formed with inorganic-polymer material pairs [33–37] and organic-polymer material pairs [15,16,19,25, 38–45], some improvements in the PF (typically small increase in the

PF) have been reported in the past. The origin of the improvement has not been discussed or has been often conjectured to be energy dependent electronic filtering without detailed experimental evidences. A recent study pointed out that the origin of the improvement in the PF of polymer composites could be attributed to the morphology changes of the polymers near the fillers [46], but it is still under debate. In this study, it should be noted that we used two separated CNT films connected by PEDOT, which is different from the commonly studied composites where mixture of polymer precursors (or polymers) and fillers are often chemically processed together to generate newly-formed, large amount of polymer/filler interfaces.

When the SWCNT-PEDOT junction is formed without any gate bias  $(V_g=0~\rm V)$ , an energy barrier for holes is present (Fig. 4b), and, as  $V_g>0~\rm V$ , the energy barrier height becomes larger (Fig. 4c). According to Eq. (1), it is estimated that  $E_{b,po}<0.13~\rm eV$  and  $E_b\sim0.13~\rm eV$  for holes. Let's reconsider the differential conductivity of CNTs (Fig. 1c) whose Fermi level is located near the band edge of s-CNT like the CNT in this experiment. The non-zero differential conductivity appears over an energy window of  $\sim0.3~\rm eV$  (Fig. 1c). Thermopower is proportional to the average value of  $E-E_f$  or the ratio of the shaded area in Fig. 1d to that in

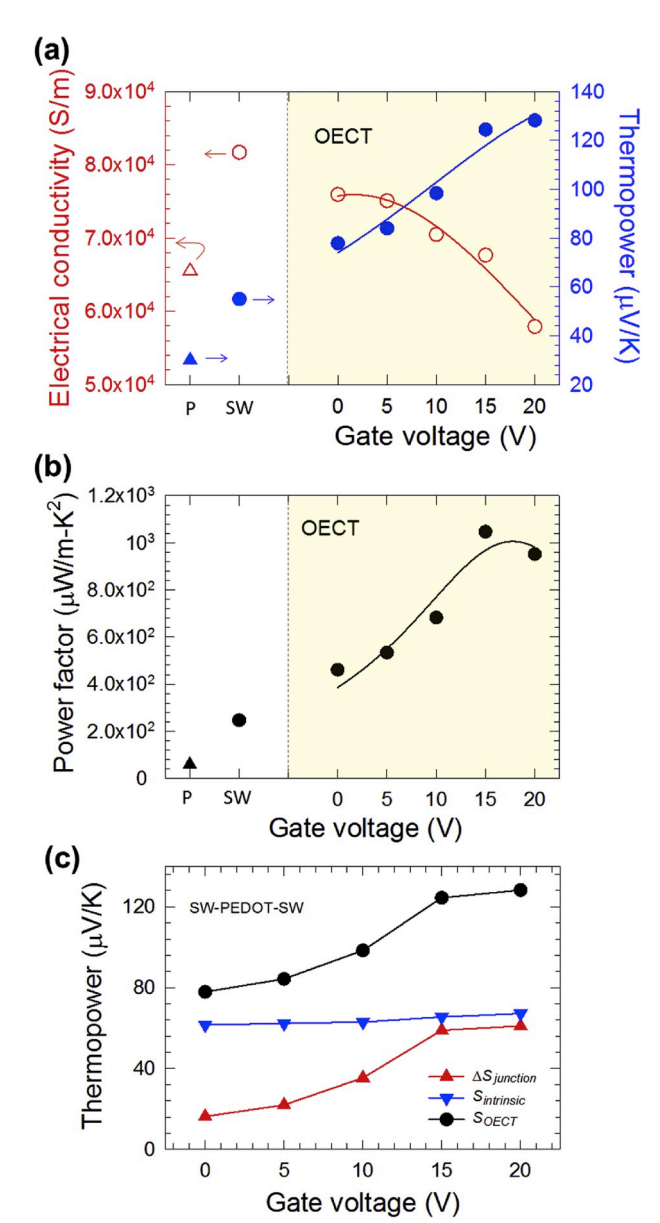


**Fig. 5.** (a) Electrical conductivity and thermopower and (b) power factor of the OECT with SWCNT as a function of gate voltage along with those of PEDOT:PSS and SWCNT (indicated by P and SW, respectively) for comparison. (c) The thermopower ( $S_{OECT}$ ) of the OECT with SWCNT was divided into two parts, contribution from the intrinsic properties ( $S_{intrinsic}$ ) of SWCNT and PEDOT:PSS and that ( $\Delta S_{junction}$ ) from the CNT-PEDOT-CNT junction when the gate voltage was varied from 0 V to 20 V.

Fig. 1c according to Eq. (1). In Fig. 1d, the negative area decreases the sum of the shaded area, and imposing an energy barrier could be represented by eliminating the shaded area in Fig. 1d. When the negative area gets smaller, the sum of the shaded areas increases (Fig. 1e), suggesting thermopower could be raised by diminishing hole transport from m-CNT to PEDOT.

The thermopower was raised and saturated at  $V_g\!=\!15\,\mathrm{V}$ , resulting in a remarkably improved PF of  $\sim\!10^3\,\mu\mathrm{W/m}\text{-K}^2$ , compared with those of individual materials (SWCNT, PEDOT:PSS) (Fig. 5b). The PEDOT:PSS-CNT junction could enable hole injection from PEDOT:PSS to SWCNT, as illustrated in Fig. 4b. As PEDOT:PSS has a larger hole carrier concentration than that of SWCNT [47], the extra holes injected to the cold side would result in a larger charge imbalance between the hot and cold sides, and thus a larger voltage difference (i.e., thermopower) could be observed.

The contribution of the gate voltage to thermopower ( $\Delta S_{junction}$ ) was further analyzed using the following relation:

$$\Delta S_{iunction}(V_g) = S_{OECT}(V_g) - S_{intrinsic}(V_g)$$
(4)

where  $S_{OECT}$  considers the energy barrier but  $S_{intrinsic}$  was obtained using a simple series circuit model of CNT and PEDOT:PSS without considering the energy barrier.  $S_{intrinsic}$  can be calculated by the sum of thermoelectric voltage generated by individual CNT and PEDOT as follows:

$$S_{intrinsic}(V_g) = \left(S_{CNT}\Delta T_{CNT} + S_{PEDOT}(V_g)\Delta T_{PEDOT}\right)/\Delta T_{CNT+PEDOT} \tag{5}$$

where  $S_{CNT}$  is the intrinsic thermopower of CNT (see Fig. 5a);  $S_{PEDOT}(V_g)$  is the thermopower of PEDOT:PSS as a function of gate voltage (Fig. S7c); and  $\Delta T$  is the temperature difference along the indexed material. The temperature differences,  $\Delta T$  s for CNT and PEDOT are proportional to the length of each material (CNT, PEDOT) as a result of a linear temperature profile along the source-to-drain direction because the CNT and PEDOT thin films are at least 3 orders of magnitude thinner than the glass substrate that were heated to create  $\Delta T$ .

 $\Delta S_{junction}$  and  $S_{intrinsic}$  along with  $S_{OECT}$  for SWCNT are shown in Fig. 5c, and those for DWCNT and MWCNT are shown in Figs. S8a and b, respectively. It is worth noting that the variation of  $S_{intrinsic}$  is small as a function of gate voltage despite the large change in  $S_{PEDOT}$  with  $V_g$  (Fig. S7c). This is because  $S_{CNT}$  is not a function of  $V_g$  and the length of PEDOT:PSS is much shorter than that of CNT. As a result,  $\Delta T_{PEDOT}$  is small in Eq. (5) so  $S_{PEDOT}\Delta T_{PEDOT}$  term becomes small. Therefore, it is clear that the improvement of thermopower for OECT ( $S_{OECT}$ ) mainly comes from the CNT-PEDOT-CNT junction.

While the OECT layout is ideal for systematic studies, it is difficult to utilize the OECT as an actual thermoelectric material or a thermoelectric device because of the externally supplied bias voltage. Here we further studied a practical configuration using a chemical reduction method for PEDOT:PSS with hydrazine instead of the bias voltage. CNT films were connected by thin PEDOT:PSS layers whose doping level was controlled by the exposure of hydrazine, and this process was repeated to fabricate multiple CNT-PEDOT:PSS junctions in series (Fig. 6a) so that hole transport occurs through multiple CNT-PEDOT:PSS-CNT junctions. The de-doping process was controlled by limiting the exposure time to hydrazine so that the doping concentration by the chemical reduction is close to that of OECT. The electrical conductivity of chemically reduced PEDOT:PSS was configured to have that of the PEDOT:PSS  $(\sim 1.45 \times 10^4 \text{ S/m})$  at  $V_g = 15 \text{ V}$ , which creates the optimum energy barrier height for maximizing the PF according to the OECT results. The adjustment of the doping level for PEDOT:PSS could be done prior to the deposition so that the hydrazine exposure becomes unnecessary. The PEDOT:PSS layers were designed to be thin (~55 nm) so that the contribution of PEDOT:PSS to the electrical conductivity is minimized.

Fig. 6b shows that thermopower was raised by adding more junctions and then became saturated at 8 junctions while electrical conductivity was gradually decreased. The gradual increase in thermopower with more PEDOT junctions in the multi-junction samples could be attributed to the much thinner PEDOT layers than the length of the OECT along the hole traveling direction. In the multi-junction samples, the carriers transport along the very thin (~55 nm) out-of-plane direction, compared with the in-plane direction (3 mm) in OECT. PEDOT:PSS is composed of two segregated parts, more electrically conducting PEDOTrich parts and more insulating PSS-rich parts [48]. In the PSS part, a portion in a form of the sulfonate unit  $(-SO_3^-)$  makes a corresponding portion of PEDOT in a doped state, and the other portion (-SO<sub>3</sub>H) does not play a role in doping [49]. In addition, the hydrazine treatment de-dope portions of PEDOT:PSS, resulting in an electrically inhomogeneous material. In our samples, the thickness of the PEDOT:PSS layer is comparable to the grain size of PEDOT, ranging from several nm to several 10's nm [50,51], in contrast to the much longer PEDOT:PSS in OECT along the in-plane direction. We conjecture that the inhomogeneous nature across the PEDOT:PSS grains creates imperfect barriers,

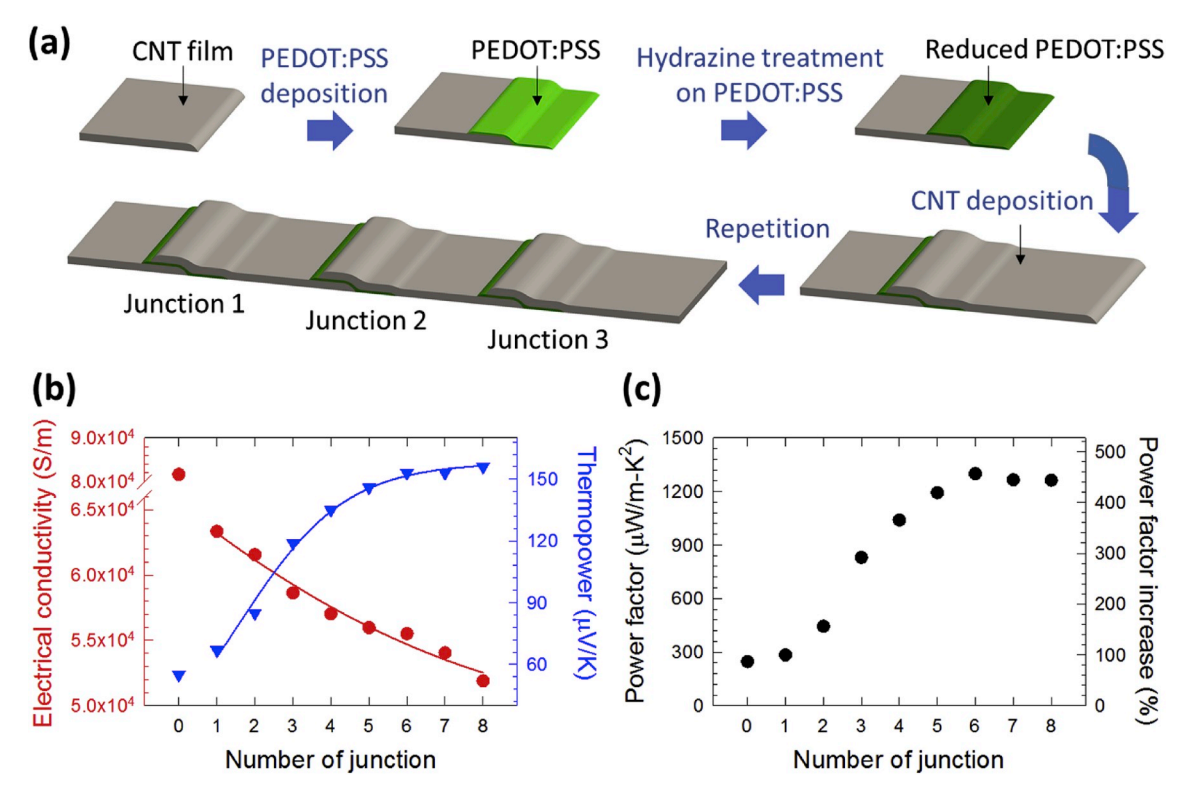


Fig. 6. (a) Fabrication process of the multiple SWCNT-PEDOT:PSS-SWCNT junctions whose PEDOT:PSS was chemically reduced by hydrazine to have the optimum doping level. Note that hole transport occurs along the thickness direction of the PEDOT layer. (b) Electrical conductivity and thermopower and (c) power factor of the multi-junction sample when the number of junction was varied from 1 to 8. The electrical properties of SWCNT were plotted together at 0 junction for comparison.

which requires multiple PEDOT:PSS junctions to raise the thermopower. With 6 junctions, the PF was remarkably enhanced to  $1.3\times10^3\,\mu\text{W/m-K}^2,$  which is  $\sim\!460\%$  improvement from the PF of the CNT only sample and the highest value for CNT films, to our best knowledge (Fig. 6c). It should be noted that this experiment has been carried out in order to demonstrate a method for implementing this concept in composites.

# 3. Conclusions

This work presents a systematic study and a practical method for improving the PF of CNT/polymer thermoelectric composites. When PEDOT:PSS connects CNT films at their junctions, the thermopower of the CNT-PEDOT-CNT films could be higher than those of individual components, CNT and PEDOT:PSS, resulting in  $\sim 1.3 \times 10^3 \, \mu \text{W/m-K}^2$ , which is the highest PF for CNT films, to our best knowledge. To study the origin of the improvement systematically, the OECT configuration with a modulated polymer (PEDOT:PSS) channel between CNTs were employed. When the junction was formed, we believe that an energy barrier was created. Then a positive gate bias voltage further raised the energy barrier height, based on the experimentally constructed band diagrams and theoretical estimation. Multiple different measurement techniques (CV, UV-vis, KPFM) were used to verify the HOMO, LUMO, and Fermi levels of CNT and PEDOT. Here the PF and thermopower improvements could be attributed to the PEDOT:PSS junction that abates the contribution of m-CNT to thermopower as well as injects holes to CNT films so that charge imbalance between the hot and cold side upon imposing temperature gradients can be enlarged for larger thermopower. For practical use without applying an external bias voltage required in OECT, multi-junction samples mimicking composite structures made of CNT and PEDOT:PSS were created. With six CNT-PEDOT connections, the thermopower was raised up to  ${\sim}150\,\mu\text{V/K}$ and a remarkably high PF was obtained up to  $\sim 1.3 \times 10^3 \,\mu\text{W/m-K}^2$ ,

which is  $\sim\!460\%$  improvement compared with that of pristine CNT and is comparable to those of inorganic counterparts. Here the doping level of PEDOT:PSS channel was chemically adjusted to match the best condition from the OECT experiment. We anticipate that this study shows a practical way of utilizing the large thermoelectric response of s-CNT by suppressing the contribution from m-CNT as well as provides insight about how the junction promotes selective hole transport. The presented method for suppressing the electronic transport from m-CNT could be widely applicable to other organic materials and composites for thermoelectrics and beyond.

#### 4. Method

To fabricate OECT, CNT solutions were prepared by mixing 10-mg of CNT with 30-mg sodium dodecylbenzenesulfonate (SDBS) and 20-g deionized (DI) water and then sonicated the mixture with a pen-type sonicator for 2h and an ultrasonic bath for 6h for dispersion. Then the source, drain, and gate CNT electrodes were prepared by spraying onto pre-cleaned glass CNT solution substrates  $(3 \text{ inch} \times 1 \text{ inch} \times 1 \text{ mm})$  masked with a Kapton tape at  $\sim 80 \,^{\circ}\text{C}$  with a spray gun to have a gap of 3 mm between the source and drain electrodes. The samples were immersed into DI water overnight for washing out excess SDBS, and then dried on a hotplate. The CNT film thickness was measured to be  $158 \pm 5$  nm. As-purchased PEDOT:PSS was mixed with 5 wt% dimethyl sulfoxide (DMSO) for doping and stirred at  $\sim$ 80 °C overnight. After removing the Kapton mask, another mask covered the CNT area, and then the gap between source and drain was bridged by spraying PEDOT:PSS (1  $\mu m \pm 50$  nm). Finally, PSSH was sprayed to make a gate insulator on top of the PEDOT and the gate electrode at room temperature.

To fabricate PEDOT/CNT multi-junction samples, CNT films were similarly prepared by the spraying method. The PEDOT:PSS solution was sprayed through a shadow mask to have an overlapped region

(~2 mm in length) with the pre-deposited CNT film (~9 mm in length). The PEDOT film thickness was measured to be  $55\pm3$  nm. The PEDOT: PSS film was then reduced by treating it with hydrazine vapor in a sealed box for 2.5 min while the CNT parts were covered by a mask. These steps were repeated until 8 PEDOT-CNT junctions were reached. The details about the measurement methods for thermopower and electrical conductivity can be found from our earlier papers [30,31]. All other measurement details and chemicals used are available in the supplementary information.

#### Acknowledgments

This research was supported by US National Science Foundation (CBET 1805963) and Creative Materials Discovery Program through the National Research Foundation of Korea (NRF) funded by Ministry of Science and ICT (2018M3D1A1057844).

## Appendix A. Supplementary data

Supplementary data to this article can be found online at https://doi.org/10.1016/j.nanoen.2019.104282.

#### References

- B. Russ, A. Glaudell, J.J. Urban, M.L. Chabinyc, R.A. Segalman, Organic thermoelectric materials for energy harvesting and temperature control, Nat. Rev. Mater. 1 (2016) 16050.
- [2] G. Chen, W. Xu, D. Zhu, Recent advances in organic polymer thermoelectric composites, J. Mater. Chem. C 5 (2017) 4350.
- [3] H. Wang, C. Yu, Organic thermoelectrics: materials preparation, performance optimization, and device integration, Joule (2018), https://doi.org/10.1016/j. joule.2018.10.012.
- [4] N. Toshima, Recent progress of organic and hybrid thermoelectric materials, Synth. Met. 225 (2017) 3.
- [5] Q. Zhang, Y. Sun, W. Xu, D. Zhu, Organic thermoelectric materials: emerging green energy materials converting heat to electricity directly and efficiently, Adv. Mater. 26 (2014) 6829.
- [6] M. He, F. Qiu, Z. Lin, Towards high-performance polymer-based thermoelectric materials, Energy Environ. Sci. 6 (2013) 1352.
- [7] R. Kroon, D.A. Mengistie, D. Kiefer, J. Hynynen, J.D. Ryan, L. Yu, C. Müller, Thermoelectric plastics: from design to synthesis, processing and structure–property relationships, Chem. Soc. Rev. 45 (2016) 6147.
- [8] A.S. Tazebay, S.-I. Yi, J.K. Lee, H. Kim, J.-H. Bahk, S.L. Kim, S.-D. Park, H.S. Lee, A. Shakouri, C. Yu, Thermal transport driven by extraneous nanoparticles and phase segregation in nanostructured Mg2(Si,Sn) and estimation of optimum thermoelectric performance, ACS Appl. Mater. Interfaces 8 (2016) 7003.
- [9] R. Kroon, D.A. Mengistie, D. Kiefer, J. Hynynen, J.D. Ryan, L. Yu, C. Müller, Thermoelectric plastics: from design to synthesis, processing and structure–property relationships, Chem. Soc. Rev. 45 (2016) 6147.
- [10] H. Wang, L. Yin, X. Pu, C. Yu, Facile charge carrier adjustment for improving thermopower of doped polyaniline, Polymer 54 (2013) 1136.
- [11] X. Crispin, S. Marciniak, W. Osikowicz, G. Zotti, A.W.D. van der Gon, F. Louwet, M. Fahlman, L. Groenendaal, F. De Schryver, W.R. Salaneck, Conductivity, morphology, interfacial chemistry, and stability of poly(3,4-ethylene dioxythiophene)-poly(styrene sulfonate): a photoelectron spectroscopy study, J. Polym. Sci. B Polym. Phys. 41 (2003) 2561.
- [12] C. Yu, L. Shi, Z. Yao, D. Li, A. Majumdar, Thermal conductance and thermopower of an individual single-wall carbon nanotube, Nano Lett. 5 (2005) 1842.
- [13] C. Yu, S. Saha, J. Zhou, L. Shi, A.M. Cassell, B.A. Cruden, Q. Ngo, J. Li, Thermal contact resistance and thermal conductivity of a carbon nanofiber, J. Heat Transf. 128 (2005) 234.
- [14] R.S. Prasher, X.J. Hu, Y. Chalopin, N. Mingo, K. Lofgreen, S. Volz, F. Cleri, P. Keblinski, Turning carbon nanotubes from exceptional heat conductors into insulators, Phys. Rev. Lett. 102 (2009) 105901.
- [15] C. Yu, Y.S. Kim, D. Kim, J.C. Grunlan, Thermoelectric behavior of segregatednetwork polymer nanocomposites, Nano Lett. 8 (2008) 4428.
- [16] C. Yu, K. Choi, L. Yin, J.C. Grunlan, Light-weight flexible carbon nanotube based organic composites with large thermoelectric power factors, ACS Nano 5 (2011) 7885.
- [17] Y. Ryu, L. Yin, C. Yu, Dramatic electrical conductivity improvement of carbon nanotube networks by simultaneous de-bundling and hole-doping with chlorosulfonic acid, J. Mater. Chem. 22 (2012) 6959.
- [18] C. Meng, C. Liu, S. Fan, A promising approach to enhanced thermoelectric properties using carbon nanotube networks, Adv. Mater. 22 (2010) 535.
- [19] H. Wang, S.-i. Yi, X. Pu, C. Yu, Simultaneously improving electrical conductivity and thermopower of polyaniline composites by utilizing carbon nanotubes as high mobility conduits, ACS Appl. Mater. Interfaces 7 (2015) 9589.

[20] K. Choi, S.L. Kim, S.-i. Yi, J.-H. Hsu, C. Yu, Promoting dual electronic and ionic transport in PEDOT by embedding carbon nanotubes for large thermoelectric responses, ACS Appl. Mater. Interfaces 10 (2018) 23891.

- [21] Y. Nakai, K. Honda, K. Yanagi, H. Kataura, T. Kato, T. Yamamoto, Y. Maniwa, Giant Seebeck coefficient in semiconducting single-wall carbon nanotube film, APEX 7 (2014), 025103.
- [22] A.D. Avery, B.H. Zhou, J. Lee, E.-S. Lee, E.M. Miller, R. Ihly, D. Wesenberg, K. S. Mistry, S.L. Guillot, B.L. Zink, Y.-H. Kim, J.L. Blackburn, A.J. Ferguson, Tailored semiconducting carbon nanotube networks with enhanced thermoelectric properties, Nat. Energy 1 (2016) 16033.
- [23] Y. Akai, S. Saito, Electronic structure, energetics and geometric structure of carbon nanotubes: a density-functional study, Phys. E Low-dimens. Syst. Nanostruct. 29 (2005) 555.
- [24] C. Yu, Y. Ryu, L. Yin, H. Yang, Modulating electronic transport properties of carbon nanotubes to improve the thermoelectric power factor via nanoparticle decoration, ACS Nano 5 (2011) 1297.
- [25] H. Wang, S.-i. Yi, C. Yu, Engineering electrical transport at the interface of conjugated carbon structures to improve thermoelectric properties of their composites, Polymer 97 (2016) 487.
- [26] N.D. Robinson, P.-O. Svensson, D. Nilsson, M. Berggren, On the current saturation observed in electrochemical polymer transistors, J. Electrochem. Soc. 153 (2006) H39.
- [27] S. Nanot, N.A. Thompson, J.-H. Kim, X. Wang, W.D. Rice, E.H. Hároz, Y. Ganesan, C.L. Pint, J. Kono, Single-Walled Carbon Nanotubes in Handbook of Nanomaterials, Springer, Berlin, 2013.
- [28] W. Shi, Q. Yao, S. Qu, H. Chen, T. Zhang, L. Chen, Micron-thick highly conductive PEDOT films synthesized via self-inhibited polymerization: roles of anions, NPG Asia Mater. 9 (2017) e405.
- [29] S. Demtchenko, N.G. Tarr, S. McGarry, Effect of PEDOT band structure on conductive polymer-insulator-silicon junctions, J. Appl. Phys. 122 (2017), 065502.
- [30] H. Wang, J.-H. Hsu, S.-I. Yi, S.L. Kim, K. Choi, G. Yang, C. Yu, Thermally driven large N-type voltage responses from hybrids of carbon nanotubes and poly(3,4ethylenedioxythiophene) with tetrakis(dimethylamino)ethylene, Adv. Mater. 27 (2015) 6855.
- [31] S.L. Kim, H.T. Lin, C. Yu, Thermally chargeable solid-state supercapacitor, Adv. Energy Mater. 6 (2016) 1600546.
- [32] S.L. Kim, J.-H. Hsu, C. Yu, Thermoelectric effects in solid-state polyelectrolytes, Org. Electron. 54 (2018) 231.
- [33] J. Choi, J.Y. Lee, S.-S. Lee, C.R. Park, H. Kim, High-performance thermoelectric paper based on double carrier-filtering processes at nanowire heterojunctions, Adv. Energy Mater. 6 (2016) 1502181.
- [34] M. He, J. Ge, Z. Lin, X. Feng, X. Wang, H. Lu, Y. Yang, F. Qiu, Thermopower enhancement in conducting polymer nanocomposites via carrier energy scattering at the organic-inorganic semiconductor interface, Energy Environ. Sci. 5 (2012) 8351.
- [35] Z. Liang, M.J. Boland, K. Butrouna, D.R. Strachan, K.R. Graham, Increased power factors of organic—inorganic nanocomposite thermoelectric materials and the role of energy filtering, J. Mater. Chem. 5 (2017) 15891.
- [36] Y. Du, S.Z. Shen, K. Cai, P.S. Casey, Research progress on polymer-inorganic thermoelectric nanocomposite materials, Prog. Polym. Sci. 37 (2012) 820.
- [37] N.E. Coates, S.K. Yee, B. McCulloch, K.C. See, A. Majumdar, R.A. Segalman, J. J. Urban, Effect of interfacial properties on polymer–nanocrystal thermoelectric transport, Adv. Mater. 25 (2013) 1629.
- [38] D. Kim, Y. Kim, K. Choi, J.C. Grunlan, C. Yu, Improved thermoelectric behavior of nanotube-filled polymer composites with poly(3,4-ethylenedioxythiophene) poly (styrenesulfonate), ACS Nano 4 (2010) 513.
- [39] Q. Yao, L. Chen, W. Zhang, S. Liufu, X. Chen, Enhanced thermoelectric performance of single-walled carbon nanotubes/polyaniline hybrid nanocomposites, ACS Nano 4 (2010) 2445.
- [40] W. Zhou, Q. Fan, Q. Zhang, L. Cai, K. Li, X. Gu, F. Yang, N. Zhang, Y. Wang, H. Liu, W. Zhou, S. Xie, High-performance and compact-designed flexible thermoelectric modules enabled by a reticulate carbon nanotube architecture, Nat. Commun. 8 (2017) 14886.
- [41] C. Meng, C. Liu, S. Fan, A promising approach to enhanced thermoelectric properties using carbon nanotube networks, Adv. Mater. 22 (2010) 535.
- [42] C. Gao, G. Chen, A new strategy to construct thermoelectric composites of SWCNTs and poly-Schiff bases with 1,4-diazabuta-1,3-diene structures acting as bidentatechelating units, J. Mater. Chem. 4 (2016) 11299.
- [43] K. Xu, G. Chen, D. Qiu, Convenient construction of poly(3,4-ethylenedioxythiophene)-graphene pie-like structure with enhanced thermoelectric performance, J. Mater. Chem. 1 (2013) 12395.
- [44] C. Cho, B. Stevens, J.-H. Hsu, R. Bureau, D.A. Hagen, O. Regev, C. Yu, J.C. Grunlan, Completely organic multilayer thin film with thermoelectric power factor rivaling inorganic tellurides, Adv. Mater. 27 (2015) 2996.
- [45] Z. Zhang, G. Chen, H. Wang, W. Zhai, Enhanced thermoelectric property by the construction of a nanocomposite 3D interconnected architecture consisting of graphene nanolayers sandwiched by polypyrrole nanowires, J. Mater. Chem. C 3 (2015) 1649.
- [46] P. Kumar, E.W. Zaia, E. Yildirim, D.V.M. Repaka, S.-W. Yang, J.J. Urban, K. Hippalgaonkar, Polymer morphology and interfacial charge transfer dominate over energy-dependent scattering in organic-inorganic thermoelectrics, Nat. Commun. 9 (2018) 5347.
- [47] J.-H. Hsu, W. Choi, G. Yang, C. Yu, Origin of unusual thermoelectric transport behaviors in carbon nanotube filled polymer composites after solvent/acid treatments, Org. Electron. 45 (2017) 182.

- [48] J.-H. Hsu, W. Choi, G. Yang, C. Yu, Origin of unusual thermoelectric transport behaviors in carbon nanotube filled polymer composites after solvent/acid treatments, Org. Electron. 45 (2017) 182.
- [49] P. Mele, D. Narducci, M. Ohta, K. Biswas, J. Morante, S. Saini, T. Endo, Thermoelectric Thin Films, Springer, 2019.
- [50] U. Lang, E. Müller, N. Naujoks, J. Dual, microscopical investigations of PEDOT:PSS thin films, Adv. Funct. Mater. 19 (2009) 1215.
- [51] A.M. Nardes, M. Kemerink, R.A.J. Janssen, J.A.M. Bastiaansen, N.M.M. Kiggen, B. M.W. Langeveld, A.J.J.M. van Breemen, M.M. de Kok, Microscopic understanding of the anisotropic conductivity of PEDOT:PSS thin films, Adv. Mater. 19 (2007) 1196